AGRÉGATS COMME PRÉCURSEURS DES NANO-OBJETS
CLUSTERS AS PRECURSORS OF NANO-OBJECTS

Cluster–cluster fusion

Eleanor E.B. Campbell [a]*, **Alexi V. Glotov** [a,1], **Andreas Lassesson** [a], **Raphael D. Levine** [b]

[a] School of Physics and Engineering Physics, Gothenburg University & Chalmers University of Technology, 41296 Gothenburg, Sweden

[b] The Fritz Haber Research Center for Molecular Dynamics, The Hebrew University, Jerusalem 91904, Israel

Abstract

An experimental study of molecular fusion in fullerene–fullerene collisions is presented and the theoretical interpretation of the cross section is reconsidered in terms of phase space arguments and competition with direct collision induced dissociation. The form and absolute magnitude of the cross sections for $C_{60}^+ + C_{70}$ (or $C_{70}^+ + C_{60}$) and $C_{70}^+ + C_{70}$ can be understood, however, the much smaller cross section for $C_{60}^+ + C_{60}$ remains a puzzle. The fragmentation behaviour of the hot fusion product is well described by a maximal entropy model indicating equipartition of the centre of mass collision energy followed by statistical fragmentation. ***To cite this article: E.E.B. Campbell et al., C. R. Physique 3 (2002) 341–352.*** © 2002 Académie des sciences/Éditions scientifiques et médicales Elsevier SAS

fullerene–fullerene collision / fragmentation

Fusion agrégats–agrégats

Résumé

Dans cet article on présente une étude expérimentale de la fusion moléculaire lors des collisions fullerene–fullerene. L'interprétation théorique de la section efficace est reconsidérée en terme d'arguments basés sur l'espace des phases et la compétition avec la dissociation directement induite par la collision. La forme et la valeur absolue de la section efficace pour les collisions $C_{60}^+ + C_{70}$ (ou $C_{70}^+ + C_{60}$) et $C_{70}^+ + C_{70}$ sont bien comprises mais la valeur bien plus faible de la section efficace trouvée pour la collision $C_{60}^+ + C_{60}$ reste intriguante. Le comportement vis à vis de la fragmentation du produit de la fusion « chaude » est bien décrit dans le cadre d'un modèle d'entropie maximum montrant l'équipartition de l'énergie dans le centre de masse, puis la fragmentation statistique. ***Pour citer cet article : E.E.B. Campbell et al., C. R. Physique 3 (2002) 341–352.*** © 2002 Académie des sciences/Éditions scientifiques et médicales Elsevier SAS

collision fullerene–fullerene / fragmentation

1. Introduction

Atomic clusters are very promising objects for studying the general dynamical behaviour of finite systems with many degrees of freedom. They present an interesting size regime, intermediate between that of

colliding atomic nuclei and macroscopic liquid droplets. In principle atomic clusters provide great flexibility in terms of the range of sizes available experimentally, the variation in binding energies and the relative ease of exploring collision energy dependencies ranging from thermal energies to keV and beyond. Theoretical investigations on cluster–cluster collisions were pioneered by Schmidt and coworkers for collisions between two small alkali clusters. Using molecular dynamics simulations, they were able to show that a number of reaction channels, analogous to the dynamics of heavy ion collisions and colliding liquid droplets were likely to appear in atomic cluster–cluster collisions such as fusion of the two clusters [1]. Unfortunately, controlled collisions between mass-selected atomic clusters under single-collision conditions are extremely difficult to study experimentally and so far such studies have only been possible for colliding carbon clusters, or fullerenes. Fullerene–fullerene collisions can be carried out with relatively little experimental effort due to the fact that molecular beams of mass-selected carbon clusters can be produced by simply evaporating purified fullerene material. The first observation of molecular fusion between fullerenes was reported in 1993 [2] and was the starting point for a series of experiments on the reaction dynamics in low energy (50 eV–6 keV) fullerene–fullerene collisions [3–8]. The experimental work was accompanied by a number of molecular dynamics simulation studies by the Schmidt group and others [9–17]. A recent review discusses the different reaction channels that have been studied in fullerene–fullerene collisions [18]. The fusion reaction between two fullerenes differs from that of heavy ion collisions or from theoretical predictions for colliding sodium clusters in some important ways. A simple intuitive line-of-centres or absorbing sphere model (see Section 3) has been successfully applied to interpret fusion cross sections in heavy ion collisions [19] and has also been invoked to interpret the cluster–cluster cross sections [18]. However, there are three major discrepancies between the experimental fullerene fusion cross sections and the predictions of the simple model: (1) the absolute magnitude of the experimentally determined cross section is much smaller than the simple model prediction, (2) the threshold behaviour has a different energy dependence and (3) the cross section drops off significantly more rapidly than predicted at high energy. The low absolute value of the cross section has been related previously to a 'bouncing off' effect observed in MD simulation trajectories [20] while the threshold behaviour has been related to a steric effect [4]. In a recent paper [8], it was shown that molecular dynamics simulations using a simple empirical 'Brenner-I' potential were able to reproduce the energetic threshold for the fusion reaction but greatly overestimated the absolute cross section value and the width of the energy window in which fusion could be detected. More sophisticated simulations using density functional theory were better able to reproduce the cross section magnitude and window. In this paper we re-examine the experimental fusion cross sections and suggest a plausible theoretical interpretation for the deviation of the experimental results from the simple line-of-centres or absorbing sphere picture. We also take a closer look at the fragmentation behaviour after fusion and compare the experimentally determined collision energy dependence of the fragmentation patterns with a simple maximum entropy model.

2. Experimental set-up

A schematic diagram of the apparatus used for these studies is shown in Fig. 1. More details have been given previously [6]. A positively charged fullerene ion beam is produced in the source vacuum chamber by evaporating fullerene powder from an oven at a temperature of about 500 °C and ionising by electron impact at 200 eV. The ions are extracted into the main scattering vacuum chamber by a pulsed electric field. The fullerene ions gain a high vibrational excitation on ionisation. The ions with desired mass-to-charge ratio are mass-selected and directed into the scattering cell. The maximum internal energy of the mass-selected projectile ions is estimated from analysis of metastable fragmentation to be on the order of 20–25 eV [6]. The scattering cell is a cylindrical oven with a circular entrance of 2 mm diameter and a horizontal exit slit of 2 mm height allowing the detection of scattered ions at laboratory angles up to 80°. Fullerene powder of high purity (commercially available, > 99.4% C_{60} or C_{70}) is evaporated inside the cell to form the target gas. The energy spread of the parent ion beam was measured to be 5% (FWHM) of the
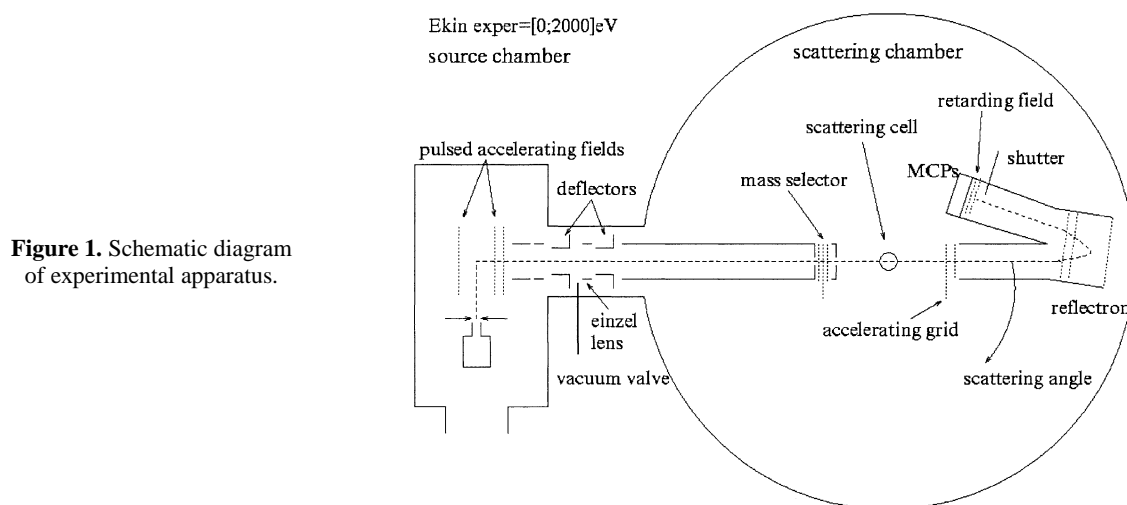
Figure 1. Schematic diagram of experimental apparatus.

laboratory collision energy, and the angular spread was measured to be $2 \pm 0.5°$ (FWHM). The positively charged products of the collision reaction are detected by a time-of-flight reflectron mass spectrometer. The reflectron can be rotated around the scattering cell allowing the determination of the angular distribution of ions. This was not considered in the early experiments [4,20] and in these papers the cross sections for fusion were underestimated at high energies where substantial fragmentation of the fusion product occurs. Newer measurements determined the angular distributions of the fusion products and integrated over these to obtain corrected values of the absolute cross sections [8]. The new, corrected values are shown in Fig. 2 (triangles), together with the original data (squares) and results of the molecular dynamics simulations, reported in [8] (circles). Note that the error bars shown are relative errors in the measurement. There is a large error with respect to the absolute cross section due mainly to uncertainty in the fullerene vapour pressure [18]. The experimentally determined threshold energy for fusion has not been affected by the corrections to the cross sections since the data close to threshold (up to ca. 100 eV) was reported accurately in the original papers. The numbers are given for convenience in Table 1. The threshold energy was determined by extrapolating the cross section to zero on a plot versus $1/E$ where E is the collision energy in the centre of mass reference frame. A linear extrapolation (in agreement with the line-of-centres model, see Fig. 3 and Section 3) does not give a very good fit to the data and hence the extracted fusion barrier energy value (E_{bfus}) has large error bars (ASM in Table 1). A better fit to the data was obtained by assuming $\sigma_{\text{fus}} \propto (E - E_{\text{bfus}})^2/E$ (SM in Table 1). Both extrapolated values are given in Table 1 along with the threshold values determined from molecular dynamics simulations. Very good agreement is found when the fusion reaction is simulated for clusters with an initial temperature of 2000 K (total $E_{\text{int}} \approx 42$ eV). This

Table 1. Cross sections for molecular fusion in fullerene–fullerene collisions

System	Experimental threshold [eV] (from [4])		Theoretical threshold [eV] (from [25])	
	ASM	SM	$T = 0$ K	$T = 2000$ K
$C_{60}^+ + C_{60}$	67 ± 7	60 ± 1	80	60
$C_{60}^+ + C_{70}$; $C_{70}^+ + C_{60}$	84 ± 9	70 ± 7	94	70
$C_{70}^+ + C_{70}$	86 ± 12	76 ± 4	104	75

ASM: from fit to experimental data using absorbing sphere or line of centres model.
SM: fit to experimental data using steric model.
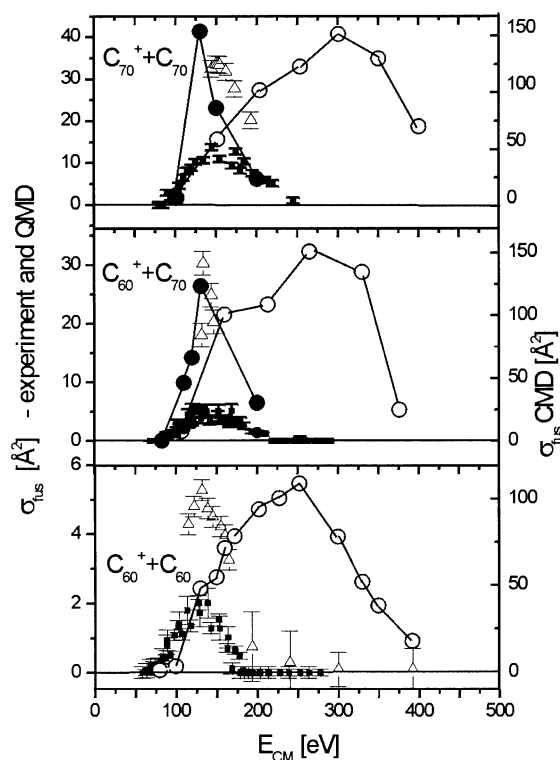Theoretical thresholds from molecular dynamics simulations.

Figure 2. Cross sections for fusion between two fullerenes: (a) $C_{60}^+ + C_{60}$; (b) $C_{60}^+ + C_{70}$ and $C_{70}^+ + C_{60}$; (c) $C_{70}^+ + C_{70}$. Squares: earlier data [4]; triangles: data corrected for fragment scattering [8]; filled circles: density functional MD calculations [8]; open circles (right hand axis) empirical potential MD calculations [8]. Adapted from [8].
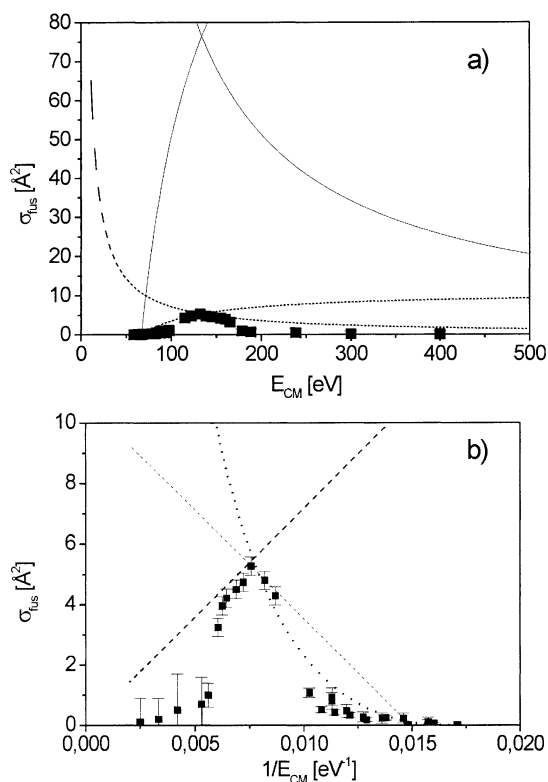
Figure 3. Experimental fusion cross section for $C_{60}^+ + C_{60}$ collisions (squares) compared with the line-of-centres cross section. (a) Plotted versus centre of mass collision energy, E_{CM}. Full line: line-of-centres model with centrifugal cut-off. Dashed line: full line scaled with an average steric factor $p = 0.07$. (b) Plotted versus $1/E_{CM}$. Dashed lines as (a), dotted line: steric model.

is probably an overestimation of the initial internal energy in the colliding clusters. In the experiments the internal energies or temperatures of the projectile and target clusters are different. The target cluster has the temperature of the target cell (773 K $\approx$ 4.5 eV) but the projectile ion is at a higher temperature, estimated to be 2000 $\pm$ 100 K ($\approx$ 21 $\pm$ 2 eV) [21] and thus close to the simulated temperature.[2]

Product ions from a fusion reaction can be easily distinguished from those from an inelastic collision if the mass of the product ion is larger than the projectile ion mass since they arrive at the ion detector at later times and do not overlap with the products of inelastic collisions. Small fragment ions are much more difficult to distinguish and tend to be masked by the projectile ion peak and fragmentation products from inelastically scattered C_{60}^+. We distinguish them by selecting product ions within a given velocity range (around half of the initial projectile ion velocity) after collision. The selected ions are accelerated with a pulsed electric field and mass selected in the reflectron. The mass and angular resolution of this method is rather poor but it does allow us to be confident of the assignments in the spectra. Details of the procedure are given in [6]. The ion intensities are corrected for the velocity-dependent detection efficiency of the channel plates [4].

344

3. Theoretical considerations

3.1. Fusion cross section

Fusion is an activated process with the energy thresholds given in Table 1. The simplest expectation is that the magnitude and energy dependence of the fusion cross section will be limited by the condition that the energy available along the line of centres of the two fullerenes exceeds this threshold. At an initial relative translational energy E and impact parameter b the energy along the line of centres is $E(1 - b^2/R^2)$ where R is the centre-to-centre distance [23]. Locating the barrier to fusion at $R = d \approx 7$ Å, the maximal impact parameter that allows the crossing of the barrier is determined by $E(1 - b_{\mathrm{m}}^2/R^2) = E_{\mathrm{bfus}}$ or

$$\sigma_{\mathrm{fus}} = \begin{cases} 0, & E \leqslant E_{\mathrm{bfus}}, \\ \pi d^2(1 - E_{\mathrm{bfus}}/E) \end{cases} \quad \text{(line of centres model).} \tag{1}$$

The actual experiment uses rather hot fullerenes that bring in lots of internal energy (ca. 25 eV, as discussed above). Molecular dynamics computations [4], quoted also in Table 1, show that the barrier height is lowered significantly by including internal energy, to a level consistent with the fitted experimental values.

The measured fusion cross section differs from the simple line of centres model in several key respects. The rise at threshold is not quite linear in $1/E$, see Fig. 3. Also the slope is quite wrong. The geometrical forefactor is nowhere near as large as πd^2. It is well known in conventional chemical kinetics that the size of the cross section is over estimated by the line of centres model. One tends to ascribe this to steric requirements of the reaction and the simplest correction is to lower the probability of reaction by a 'steric factor' p, $p < 1$. The forefactor is then $\pi d^2 p$ and fitting values of p to the experimental data (corrected for scattering losses, Fig. 2 [8]) yields values from 0.07 for fusion in $C_{60}^+ + C_{60}$ collisions to 0.4 for $C_{60}^+ + C_{70}$ or $C_{70}^+ + C_{60}$ and 0.45 for $C_{70}^+ + C_{70}$ collisions. A more refined approach makes the steric constraint depend also on the impact parameter but to compute it requires knowledge of the barrier as a function of the approach geometry. In earlier work, the experimental data was fitted with a $(E - E_{\mathrm{bfus}})^2/E$ dependence which implies that the steric factor, p, rises linearly with collision energy [24]. This could be rationalised if different relative orientations of the fullerenes on impact have different fusion barriers. However, density functional computations do not support a strong dependence of the barrier on the detailed geometry of the two fullerenes at the moment of impact [21] although the calculated fusion probability is significantly lower than the simple model predictions and in good agreement with the experimental data, Fig. 2. The dependence on the initial orientation was tested in two different ways. First, two C_{60} were oriented hexagon-to-hexagon (6×6) or pentagon-to-pentagon (5×5). Then one of the fullerenes was rotated around the collision axis by the angle $\delta\theta$. The collision trajectory was calculated for each value of $\delta\theta$ and for several collision energies. The probability for fusion was found to be much more dependent on the collision energy close to threshold than on the initial orientation [21]. No correlation with orientation could be found. Secondly, the principal orientation of C_{70} was chosen [25] prior to $C_{70} + C_{60}$ collisions. The simulations showed no dependence on the orientation of the symmetry axes of C_{70}. For $C_{60} + C_{60}$ there are unfortunately not enough trajectory calculations using the density functional approach to estimate the fusion cross section. An early report gave an average calculated fusion probability for $C_{60} + C_{60}$ close to threshold of 0.06 [20].

Beyond the threshold regime the measured fusion cross section declines quite steeply with increasing collision energy, say from about 150 eV on, Figs. 2 and 3. In nuclear physics this decrease in the probability of fusion is associated with the compound nucleus not being formed because if it were, the rotational energy will be above the stability line. In other words, the impact parameter is so high that the effective potential $V(R) + Eb^2/R^2$ no longer supports a well. Taking the case of $C_{60}^+ + C_{60}$, the estimated stability of the peanut shaped isomer of C_{120}^+ is about that of the reactants [26]. So C_{120}^+ has a barrier for dissociation which is the fusion barrier whose height is about 80 eV. To fill-in the well to the left of the barrier at, say, $R = 7$ Å and a collision energy of 150 eV requires impact parameters above 5 Å. The energy dependence

of the cross section due to such a cutoff is

$$\sigma_{\text{fus}} = \pi R^2 (E_{\text{bfus}}/E) \quad \text{(centrifugal cutoff for } E > E_{\text{bfus}}\text{).} \tag{2}$$

Here too, the forefactor is way too large and the decrease as 1/energy is too moderate to fit the steep drop of the cross section, Fig. 3.

In view of the qualitative discrepancies with two-body models we discuss an alternative interpretation of the fusion channel. It is consistent with both the experimental observations and the molecular dynamics simulations for both an empirical and a density-functional based potential [8]. The proposed interpretation is based on there being alternative reaction channels and that these take away flux that could otherwise reach the fusion channel. To follow the argument it is necessary to keep in mind that the experimental criterion for fusion is that a large (50%) fraction of the initial laboratory collision energy has been dissipated and that there is no centre of mass motion after reaction. [3]

In the post-threshold regime we consider that the fusion channel is the minority player. A much more probable outcome of the collision are quasi-elastic and inelastic events where one fullerene acquires a small but finite fraction of the collision energy as internal excitation and the other one remains more or less as hot as it were. We argue that in the threshold regime the available phase space for this inelastic channel is larger than that for the formation of a very hot compound fullerene, say C_{120}^+.[4] Such a competing channel was observed in molecular dynamics simulations and discussed in terms of a 'bouncing off' process [20].

To estimate the branching ratio we require the density of vibrational states of a polyatomic molecule. For our purpose the simple RRK estimate is sufficient because we only need ratios and not absolute numbers. For an n-atomic species with s vibrational modes, $s = 3n - 6$, and a (geometric) mean vibrational frequency $\overline{\nu}$ ($2.7 \cdot 10^{13}$ Hz $= 900$ cm^{-1} for C_{60}) the number of vibrational states below the energy E is

$$N(E) = \frac{1}{s} \left(\frac{E}{h\overline{\nu}} \right)^s \quad \text{(harmonic count).} \tag{3}$$

The Stirling approximation $s! \approx \sqrt{2\pi s}(s/\text{e})^s$ allows us to focus attention on the variable of interest namely $(E/h\overline{\nu})/(s/\text{e}) = \text{e}(E/sh\overline{\nu})$. When this variable exceeds unity, we are in the vibrational quasicontinuum where the density of states is exponentially large. The essential difference between the two channels is that C_{120} has (about) 6 times as many vibrational modes as does C_{60}. Once the energy is high enough to reach the vibrational quasi-continuum of C_{120}, it will have overwhelmingly more states than C_{60}. But it takes less energy to reach the quasi-continuum of C_{60}.[5] In the immediate post threshold region we thus expect that many collisions do not end up in fusion but in inelastic collisions. At higher energies the situation is reversed and, because of the steep rise of the density of states with energy, once formation of C_{120} is the dominant channel, it is the overwhelmingly dominant one. This very simple consideration leads to a much steeper rise of the cross section close to threshold. The increasing phase space that becomes available for fusion at energies past the barrier means that the fusion cross section rises more rapidly than as $1 - E_{\text{bfus}}/E$, as seen in Figs. 2 and 3. Examples are shown in Fig. 4 based on the cross section for fusion in $C_{70}^+ + C_{70}$ collisions (with $E_{\text{bfus}} = 100$ eV). The line-of-centres cross section is given by the dashed line. The full lines have been calculated assuming two different values for the internal energy of the collisionally excited fullerene: 5 eV and 20 eV. In both cases it was assumed that 30% of the centre of mass collision energy was converted to vibrational excitation of the scattered fullerene, in agreement with experimental results [6]. Using this simple picture, the cross section rises steeply at threshold and has positive curvature, in agreement with the experimental results. It still does not follow the experimental data very closely due to the abrupt take-over of the C_{120} channel and rises more steeply than experiment. In the experiment there is a broad range of initial internal excitation energies of the projectile and target fullerenes and also a range of collisional energy transfer in the inelastic collisions. We believe that by taking these factors properly into account the agreement with experiment in the threshold region would be greatly improved. Unfortunately,

Figure 4. Effect of scattering channel on fusion threshold region. Parameters for $C_{70}^+ + C_{70}$ collisions. Dashed line: line-of-centres model. Full lines: cross section considering the branching ratio between fusion and scattering for two values of the initial (pre-collision) internal energy of C_{60}. For this estimate a collisional energy transfer of $0.3 E_{CM}$ was assumed.
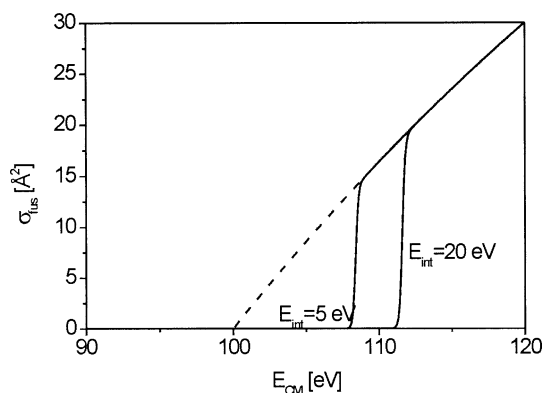
the form of the internal energy distribution and the details of the collisional energy transfer are unknown and for this reason we have refrained from a more detailed analysis.

Fusion is operationally defined as formation of a compound species accompanied by an extensive dissipation of the internal energy. It is however possible for the hot compound species to fragment promptly. This process is very clearly seen in molecular dynamics simulations where many trajectories leading to C_{120} formation also show it breaking apart in one or two vibrations. For such short times energy is not fully dissipated and these events are not detected in the experiments as 'fusion'.

The competition with the prompt fragmentation (with incomplete energy equilibration) means that the fusion cross section will decrease strongly with energy, past the threshold for three-particle production. What we therefore require is the cross section for direct collision induced dissociation (CID). By 'direct' we mean that it is prompt and therefore involves no loss of kinetic energy except for that needed to overcome the threshold for three-particle production. The CID cross section can be computed if all the excess energy is disposed of as kinetic energy of the three outgoing particles. The result is [27]

$$\sigma_{CID} = A \frac{(E - E_{CID})^{2.5}}{E} \tag{4}$$

where A is a geometrical factor[6] and E_{CID} is the threshold for CID via fusion. The branching ratio for fusion is $(\sigma_{com} - \sigma_{CID})/\sigma_{com}$ where σ_{com} is the cross section for complex (= compound species) formation, given by the capture cross section of Eq. (1). The fusion cross section is

$$\sigma_{fus} = \sigma_{2\text{-body}}\big((\sigma_{com} - \sigma_{CID})/\sigma_{com}\big) \tag{5}$$

where $\sigma_{2\text{-body}}$ incorporates the centrifugal cut-off, Eq. (2) and accounts for the competition with scattering close to threshold. The rapid decline of the fusion cross section beyond E_{CID} as given by Eq. (5) is in good agreement with the experimental results. It is not in agreement with molecular dynamics computations if all trajectories that lead to C_{120} formation are counted. But if the very short living specie (< 2 ps) are excluded (as they have been in Fig. 2 [8]) then the molecular dynamics computations can recover the steep drop of the fusion cross section [8]. Comparison with the experimental cross sections for $C_{70}^+ + C_{70}$ and $C_{60}^+ + C_{60}$ collisions is shown in Fig. 5. The thin full line in Fig. 5(a) shows the cross section obtained from considering the capture cross section of Eq. (1) combined with the centrifugal cut-off (Eq. (2)), with $E_{bfus} = 100$ eV. The dashed line shows the scaling of the capture cross section by the average steric factor, $p = 0.45$ and has $E_{bfus} = 86$ eV. The thick full line corresponds to Eq. (5) with $E_{bfus} = 100$ eV and a threshold for collision induced dissociation via fusion, $E_{CID} = 105$ eV. The agreement with the absolute magnitude and the form of the experimental cross section is very good. Similar considerations have been made for collisions $C_{60}^+ + C_{60}$ in Fig. 5(b). The dashed lines again show the scaling of the capture cross
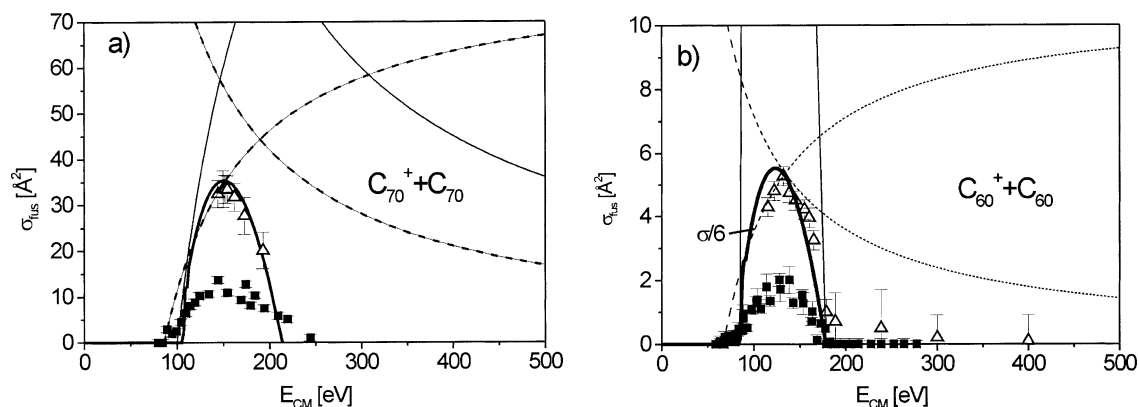
347

Figure 5. Comparison of experimental cross section with fusion models. Squares: original experimental data without correction for scattering loss; triangles: corrected fusion cross section data [8]. (a) $C_{70}^+ + C_{70}$. Thin full line: line-of-centres model with centrifugal cut-off ($E_{bfus} = 100$ eV). Dashed line: line-of-centres model ($E_{bfus} = 86$ eV) scaled with $p = 0.45$. Thick full line: fusion cross section with competing collision induced dissociation channel ($E_{bfus} = 100$ eV, $E_{CID} = 105$ eV). (b) $C_{60}^+ + C_{60}$. Dashed line: line-of-centres model scaled with $p = 0.07$ ($E_{bfus} = 67$ eV). Thin full line: fusion cross section with competing collision induced dissociation channel ($E_{bfus} = 80$ eV, $E_{CID} = 90$ eV). Thick full line: fusion cross section $\times 1/6$.

section by the average steric factor, this time $p = 0.07$ and with $E_{bfus} = 67$ eV. The thin full line corresponds to Eq. (5) with $E_{bfus} = 80$ eV and a threshold for collision induced dissociation via fusion, $E_{CID} = 90$ eV. The CID threshold has been scaled for the same impact velocity as in the $C_{70}^+ + C_{70}$ collisions and the geometrical factor A has been scaled by the reduced mass. The absolute magnitude of the cross section is much larger than that measured in the experiments (and comparable to that of $C_{70}^+ + C_{70}$) although the collision energy dependence is rather good. Satisfactory agreement with experiment can only be obtained by scaling the magnitude of the cross section down by a factor of 6, Fig. 5(b).

It is not clear to us why the fusion cross section at the maximum is so much lower for $C_{60}^+ + C_{60}$ collisions than for $C_{60}^+ + C_{70}$ or $C_{70}^+ + C_{60}$ which is a shade lower than that for $C_{70}^+ + C_{70}$ collisions. The threshold for CID should be comparable for the four possible systems. Increasing the CID cross section for $C_{60}^+ + C_{60}$ will not help since it will serve mainly to reduce the width of the cross section rather than the overall magnitude. The experiments have been reproduced a number of times and there is no reason for discrimination against the products of the $C_{60}^+ + C_{60}$ collision compared to the other reaction partners so that we can also be confident in ruling out an experimental artefact. There must be additional channels competing with fusion in the $C_{60}^+ + C_{60}$ collisions. This could be related to the rapid break-up of a dimer precursor to fusion in the $C_{60}^+ + C_{60}$ case which can be more easily stabilised leading to efficient energy dissipation and fusion for the larger collision systems. However, it is difficult to see how this would give a constant factor multiplying the cross section over the collision energy range of interest.

3.2. Fragmentation of fusion product

At collision energies slightly above threshold, the fusion product can fragment on the microsecond time scale of the experiments [6]. The average fragment ion mass and the range of fragment ions produced from the fusion product of $C_{60}^+ + C_{60}$ collisions is plotted in Fig. 6 as a function of internal energy (centre of mass collision energy plus 25 eV initial internal thermal energy). We use the procedure of maximal entropy to characterize the outcome of the collision at those higher energies. These products are operationally classified as coming from fusion because they result from a process where the initial centre of mass energy has been lost. This point is important because one implication of the procedure of maximal entropy is that
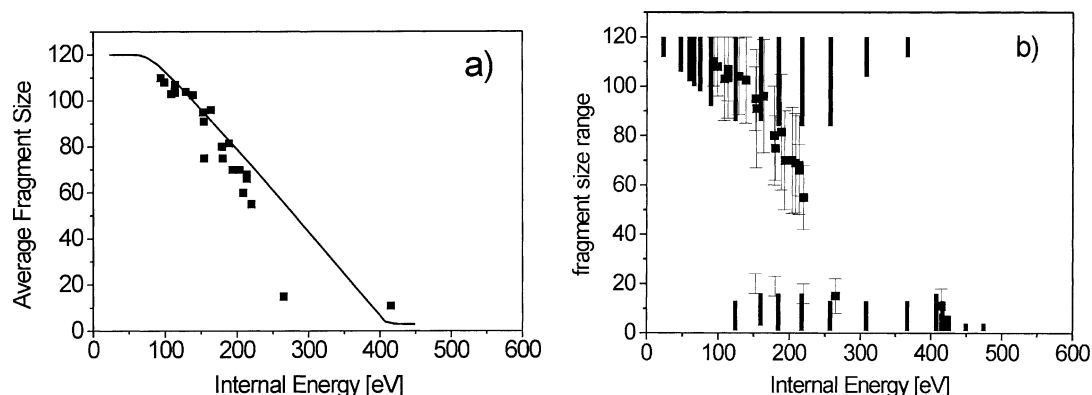
Figure 6. (a) Average fragment size from the fusion product in $C_{60}^+ + C_{60}$ collisions versus total internal energy (centre-of-mass collision energy plus initial internal energy of projectile and target). Squares: experiment data. Full line: results of maximal entropy calculation. (b) Fragment size distribution as a function of total internal energy. Squares: experimental data, thin lines indicate range of fragment sizes, not error bars. Thick lines: maximal entropy calculations.

the available energy (= collision energy + initial internal thermal energy) is equipartitioned amongst all the degrees of freedom. The technical details of the procedure are those already described for the discussion of the fragmentation of (very) energy rich C_{60} or C_{60}^+ [28]. Of course, we here apply it to (very) energy rich C_{120}^+ (or C_{130}^+ or C_{140}^+) and this means that the number of C atoms and list of possible fragments need to be suitably adjusted. The application of the maximal entropy model to the products of collisional fusion is much easier than for laser or collisional excitation of C_{60} [28] since we have a much better knowledge of the total internal energy of the fusion product. The centre of mass collision energy plus the initial vibrational excitation of the projectile ion and neutral target give the total internal energy.

One practical point is the choice of zero of energy which here needs to correspond to the experimental choice, namely internally cold C_{60} and C_{60}^+ far apart and at no relative velocity.

It is perhaps worthwhile to emphasise that the fragmentation pattern determined by the procedure of maximal entropy is based on seeking that distribution of products that corresponds to the largest volume in the accessible phase space. That means, the largest number of quantum states that it is possible to populate under the constraints of conserving energy, C atoms and charge. Any particular species has a large number of quantum states associated with it and therefore its probability is determined by counting these states. These are the states of the translation of the centre of mass. There are states associated with the internal motions about some equilibrium geometry, which is a minimum in the potential energy, and there are the different minima that we also call 'isomers'. At lower energies, it is energy (rather than entropy) that is the important variable. The reason is that it takes energy to form products that have a high energy threshold. The energy spent to overcome this threshold is not therefore available to populate high translational motion or high internal excitation or higher energy isomers. Therefore, these species have a limited number of accessible quantum states and their probability will be low. At high energy, entropy wins. Entropy favours having as many small fragments as possible because of the high number of states associated with their centre of mass motion. The computed distribution is obtained as a balance between the two opposing tendencies. The competition between these two trends is so extreme that the swing from mainly large to mainly small fragments is robust and not very sensitive to assumptions made for the purpose of counting quantum states.

One technical comment is needed about the counting of possible isomers. In our work on fragmentation of energy rich C_{60} or of C_{60}^+ we used a theoretical count of the isomers. Here we need to go up to higher fullerenes, C_{120}^+ (or C_{130}^+ or C_{140}^+), for which such input is not available. We therefore used a fit to the

number of isomers of a cluster of n atoms, of the form $\exp(-5.75 + n)$. The theory [29] suggests that the exponential increase is a shade faster than linear, but already with this form there are so overwhelmingly many ($\exp(-5.75 + 120) = 4 \cdot 10^{49}$) isomers of the parent and other large fullerenes that it really stacks the deck against fragmentation to small fragments. Yet the transition does occur, Fig. 6, because the translational entropy is also exponentially large so that what matters is the value of the exponent and not the value of the exponential. In fact, the results are not very sensitive to the expression used to estimate the number of isomers of a particular cluster size and, as discussed above, it is the binding energies and ionisation potentials of the fragment ions that have a larger influence on the outcome of the calculations.

We use the same values of the binding energies and ionisation potentials for all possible fragments up to and including C_{60} as used in our earlier work and scale the volume parameter to account for the larger size of the parent cluster [28]. Extrapolation to larger clusters is done by using the following expressions for the binding energy ($BE(n)$) and ionisation potential ($IP(n)$) of cluster n (in eV)

$$BE(n) = -7.30n + 20.241, \tag{6}$$

$$IP(n) = 5.6 + 13.8/\sqrt{n}. \tag{7}$$

These expressions are based on [30] but we have slightly reduced the binding energy of the larger clusters to obtain a smoother dependence of binding energy on n going from $n < 60$ to $n > 60$.

The comparison of the experimentally determined average fragment mass as a function of internal energy ($E + E_{\text{int}}$) with the results of the maximal entropy calculations are shown in Fig. 6(a). The agreement is very good. We show the range of detected fragment ions in Fig. 6(b). The detection limit for fragments predicted by the calculations was taken to be 0.001 (i.e. if the predicted fragment ion intensity was less than 10^{-3} of the initial parent ion intensity it was not counted). The agreement here is not quite so good. The behaviour at low collision energies follows the experiments very well and the onset of the bimodal fragment distribution is in good agreement. The main discrepancy is that the model shows the presence of C_{120}^+ up to high collision energies beyond the onset of the bimodal fragment distribution. This is not seen in the experiments where there is a steady decrease in the size of the fullerene-like fragments up to a total internal energy of ca. 200 eV. This is perhaps not too surprising. The binding energy values in the calculations are those of the most stable fullerene isomers. As discussed in Section 3.1, the product that is formed in the $C_{60}^+ + C_{60}$ collisions is not the most stable isomer of C_{120}^+ but is the 'peanut' isomer with a binding energy close to that of the reactants [26]. Fig. 7 shows the results of the maximal entropy calculation assuming that the binding energy of the largest clusters ($n > 100$) is not that of the most stable isomer. The binding energy
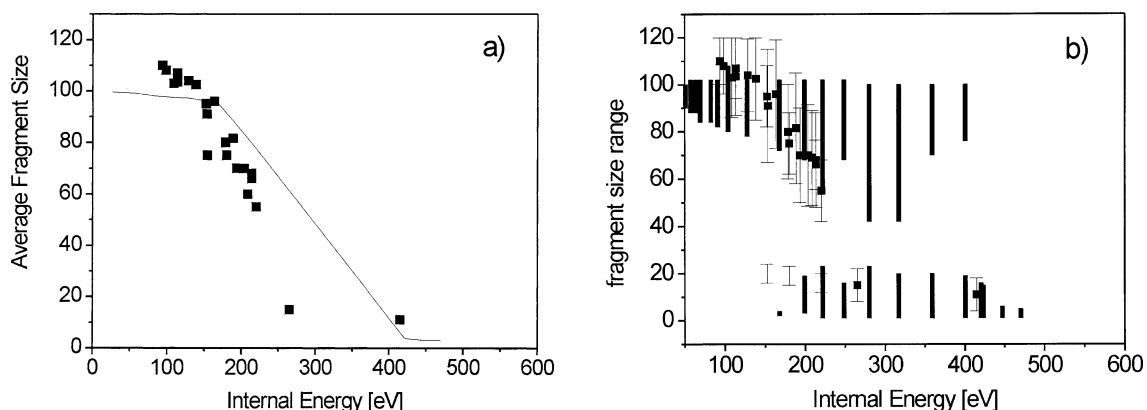

Figure 7. As for Fig. 6 but with the binding energies of the largest clusters ($n > 100$) reduced to agree better with the expected binding energies of the fusion products (less strongly bound than the most stable isomers).
$$BE(n) = -7.30n + 20.241 + 19.76(n - 100)/20.$$

of C_{120}^+ is taken to be that of the reactants and the binding energies of the fragments are adjusted to smoothly approach the binding energy of the most stable isomer for $n = 100$. This provides better agreement for the range of fragment masses as a function of internal energy (Fig. 7(b)). This is particularly so, since the intensity of the large fragments beyond ca. 250 eV internal energy is rather low and could probably not be detected above the noise level in the experiments. However, the comparison of the average fragment masses is not quite so good in Fig. 7(a) as in Fig. 6(a).

Overall, the agreement between the experimental results and the maximal entropy model is very good. This provides us with a nice confirmation that there is equilibration of the centre of mass collision energy among all the degrees of freedom of the fusion collision product and that the subsequent fragmentation behaviour is completely statistical in nature. This provides strong support for the assumptions made in analysing the angular dependence of the fragmentation in a recent study [6].

4. Conclusions

We have reconsidered the theoretical interpretation of the cross sections for molecular fusion in fullerene–fullerene collisions. The form of the cross sections close to threshold is explained in terms of a phase space argument for the competition between fusion and scattering. The magnitude and form of the cross section for $C_{60}^+ + C_{70}$ or $C_{70}^+ + C_{60}$ and $C_{70}^+ + C_{70}$ collisions can be very satisfactorily explained by invoking a competing reaction channel, direct collision induced dissociation (3-particle break-up) via fusion, at high energies. The cross section for C_{120}^+ formation in $C_{60}^+ + C_{60}$ collisions remains an enigma. It is much smaller than the models predict and there must be an additional competing channel that is only significant for these collision partners.

The experimentally determined fragmentation of the hot fusion product can be very well described within the context of a maximal entropy model, indicating equipartition of the entire centre of mass collision energy among the degrees of freedom of the fusion product followed by completely statistical fragmentation.

---

[1] Present address: Operative Elektroniksysteme, T-Systems GEI GmbH, 70771 Leinfelden-Echterdingen, Germany.

[2] Note that the estimation of the experimental temperature involved an analysis of the rate constant for metastable fragmentation of the hot fullerene projectile ion and thus depends on the model parameters used to describe this decay channel. Our estimate is based on an activation energy for C_2 loss of 10 eV and a pre-exponential factor of 10^{21} Hz [22].

[3] The large dissipation of energy must be accompanied by a similarly large dissipation of angular momentum. So the forces must have a large anisotropic component. The reason being that the high mass and high relative kinetic energy mean that even for nearly head-on collisions the orbital angular momentum l is rather high. In fact, it is so unusually high that it is worth estimating l from the standard relation [23] between it and the impact parameter b, $l = \mu v b$. Here v is the relative velocity so that, in terms of the initial kinetic energy $E = \mu v^2/2$, $l^2 = 2\mu E b^2$. It is easiest to compute in atomic units so that l comes out directly as the angular momentum quantum number. The reduced mass for a $C_{60}^+ + C_{60}$ collision in atomic mass units is $(60 \cdot 12/2) \cdot 1840 = 0.66 \cdot 10^6$ amu. Hence for energy measured in eV, and b in au of length

$$l = 155 b \, (\text{au}) \sqrt{E \, (\text{eV})}.$$

So $l \cong 1500$ already for an energy of 100 eV and an impact parameter of 1 au.

When the final relative kinetic energy is 50% or less of its initial value, there must be a corresponding large reduction in the orbital angular momentum in the exit channel.

[4] When you want to make an omelette from two eggs, you can try to smash one against the other. If you do this one egg will break but not the second one. The second egg has to be broken on the edge of the frying pan. A similar effect can also be sometimes seen in the molecular dynamics simulations of fullerene collisions.

[5] In detail, at the same internal energy one has that

$$N_{60}(E)/N_{120}(E) \approx \left(\frac{eE}{sh\overline{v}}\right)^s \bigg/ \left(\frac{eE}{2(s+3)h\overline{v}}\right)^{2(s+3)}, \quad s = 174.$$

Very approximately,

$$N_{60}(E)/N_{120}(E) \approx \left(\frac{4sh\overline{v}}{eE}\right)^{s+3}, \quad s = 174;$$

E/s is the mean energy per vibrational mode. It needs to about exceed the mean vibrational spacing, $h\overline{v} = 0.11$ eV, for C_{120} to offer more vibrational states to accommodate the internal energy. Since fusion is defined as loss of at least 50% of the initial centre of mass energy, fusion begins to dominate at collision energies on the order of 100 eV.
[6]

$$A = \frac{\pi}{60}\left(\frac{\hbar^2}{2\mu_{(2)}}\right)\left(\frac{2\mu_{(3)}d^2}{\hbar^2}\right)^{5/2},$$

where $\mu_{(2)}$ is the reduced mass, and $I^* = \mu_{(3)}d^2$ is the critical value of the moment of inertia at a configuration characterised by the generalised separation d [27].

References

[1] R. Schmidt, H.O. Lutz, Phys. Rev. A 45 (1992) 7981.
[2] E.E.B. Campbell, V. Schyja, R. Ehlich, I.V. Hertel, Phys. Rev. Lett. 70 (1993) 263.
[3] E.E.B. Campbell, F. Rohmund, A. Glotov, Nuovo Cimento 110A (1997) 1191.
[4] F. Rohmund, A.V. Glotov, K. Hansen, E.E.B. Campbell, J. Phys. B. 29 (1996) 5143.
[5] A.V. Glotov, F. Rohmund, E.E.B. Campbell, in: Y. Abe, S.-M. Lee (Eds.), Int. Symp. on Similarities and Differences Between Atomic Nuclei and Microclusters: Unified Developments for Cluster Sciences, 1997.
[6] A.V. Glotov, E.E.B. Campbell, Phys. Rev. A 62 (2000) 033202.
[7] A.V. Glotov, E.E.B. Campbell, Chem. Phys. Lett. 327 (2000) 61.
[8] A.V. Glotov, O. Knospe, R. Schmidt, E.E.B. Campbell, Eur. J. Phys. D 16 (2001) 33.
[9] O. Knospe, R. Schmidt, in: J. Jellinek (Ed.), Theory of Atomic and Molecular Clusters, Springer-Verlag, 1997.
[10] L. Liu, K. Chen, Y. Li, Chin. Phys. Lett. 10 (1993) 720.
[11] D.H. Robertson, D.W. Brenner, C.T. White, J. Phys. Chem. 99 (1995) 15721.
[12] D.H. Robertson, D.W. Brenner, C.T. White, Mat. Res. Soc. Symp. Proc., Vol. 359, 1995, p. 199.
[13] R. Schmidt, J. Schulte, O. Knospe, G. Seifert, Phys. Lett. A 194 (1994) 101.
[14] J. Schulte, Int. J. Mass Spec. Ion Proc. 145 (1995) 203.
[15] Y. Xia, Y. Xing, C. Tan, L. Mai, Phys. Rev. B 52 (1995) 110.
[16] Y. Xia, Y. Mu, C. Tan, Y. Xing, H. Yang, Nucl. Instrum. Methods Phys. Res. B 129 (1997) 356.
[17] B.L. Zhang, C.Z. Wang, C.T. Chan, K.M. Ho, J. Phys. Chem. 97 (1993) 3134.
[18] F. Rohmund, E.E.B. Campbell, Rep. Prog. Phys. 63 (2000) 1061.
[19] R. Bock (Ed.), Heavy Ion Collisions, Vols. 1–3, North-Holland, Amsterdam, 1980.
[20] F. Rohmund, E.E.B. Campbell, O. Knospe, G. Seifert, R. Schmidt, Phys. Rev. Lett. 76 (1996) 3289.
[21] A.V. Glotov, Dissertation, Göteborg University, Sweden, 2000.
[22] C. Lifshitz, Int. J. Mass Spec. 198 (2000) 1.
[23] R.D. Levine, R.B. Bernstein, Molecular Reaction Dynamics and Chemical Reactivity, Oxford University Press, New York, 1987.
[24] E.E.B. Campbell, F. Rohmund, Rep. Prog. Phys. 63 (2000) 1061.
[25] O. Knospe, A.V. Glotov, G. Seifert, R. Schmidt, J. Phys. B 29 (1996) 5163.
[26] D.L. Strout, R.L. Murry, C. Xu, W.C. Eckhoff, G.K. Odom, G.E. Scuseria, Chem. Phys. Lett. 214 (1993) 576.
[27] R.D. Levine, R.B. Bernstein, Chem. Phys. Lett. 11 (1971) 552.
[28] E.E.B. Campbell, T. Raz, R.D. Levine, Chem. Phys. Lett. 253 (1996) 261.
[29] T. Raz, U. Even, R.D. Levine, J. Chem. Phys. 103 (1995) 5394.
[30] G. Seifert, R. Gutierrez, R. Schmidt, Phys. Lett. A 211 (1996) 357.